SIMPLICITY, RIGOR AND RELEVANCE IN FLUID MECHANICS
F. J. Higuera, J. Jiménez and J. M. Vega (Eds.)

THE FLOW FIELD IN THE SLENDER COMBUSTION CHAMBERS OF SOLID PROPELLANT ROCKETS

A. Liñán
E.T.S.I. Aeronáuticos
UPM
Pza. Cardenal Cisneros 3
28040 Madrid
Spain

V. Kurdyumov
Depto. de Combustibles
Fósiles
CIEMAT
Avda. Complutense 22
28040 Madrid
Spain

J. Soler
Depto. de Matemática Aplicada
Facultad de Ciencias
Universidad de Granada
Avda. Fuentenueva s/n
18071 Granada
Spain

Abstract. We analyse the near inviscid flow field generated in a slender non-axisymmetric cylindrical cavity by the gasification and combustion reactions of a surrounding solid propellant grain. These reactions are confined to a thin layer adjacent to the surface of the solid propellant, so that the flow is non-reacting in most of the cavity, and of the same form as the flow in slender ducts due to fluid injection through lateral porous walls.

The non-reacting flow can be described in terms of self-similar solutions of the Navier -Stokes equations that we calculate numerically for star-shaped grain configurations, with Reynolds numbers only moderately large for the flow to remain laminar and steady. The self-similar flows for non-axisymmetric configurations show strong axial vortices that we analyze using the Euler simplified form of the flow equations for large Reynolds numbers, and the general solution of the Burgers equation for strained vortices that describes their viscous cores; a logarithmic singularity could then be encountered at their center lines .

Key words: flows with vorticity, solid propellant rockets, flow singularities.

1. INTRODUCTION

The purpose of this paper is to contribute to the description of the flow in the cylindrical chamber of a slender solid propellant rocket, in the fairly common case when the solid propellant, surrounding the gaseous cavity, is star-shaped, not axisymmetric.

The combustion of a solid propellant is the result of gasification reactions, often after decomposition reactions in a thin layer adjacent to the gas-solid interface, and followed by exothermic gas phase reactions which also take place in a thin reaction layer. As a consequence of these reactions, a gas flow normal to the solid surface is seen to emerge from the thin reaction layer into the cavity, with a constant

temperature T_b and a velocity U_b that depends on the local gas pressure p. The Mach number of the transverse velocity components, which are of order U_b, is very small compared with unity. The longitudinal component of the velocity, although larger than U_b by a factor of order L/a, the ratio of the chamber length L to the characteristic dimension a of the cross-section of the cavity, is still small compared with the sound speed. This is true even in cases when $L/a \gg 1$, corresponding to the slender solid propellant rockets which we consider in this paper.

If the Mach number of the gas flow is small, the spatial variations of the pressure, of order $(M_b L/a)^2$ when measured with the pressure itself, are small. As a consequence, we can consider the flow to be incompressible, with a constant value for the gas density ρ_b; in addition, the gasification velocity U_b will be considered to be constant because its variations along the surface of the propellant are also small. Our analysis will be carried out for the typical cases in which the Reynolds number $Re = U_b a/\nu_b$, based on the kinematic viscosity ν_b of the combustion gases, is large compared with unity.

The flow that we analyse is equivalent to the incompressible flow within an slender chamber bounded by porous walls through which fluid is injected into the chamber. This flow was first discussed, for large Reynolds numbers, by G.I. Taylor [1], who showed that the inviscid flow is rotational.

Culick [2] analyzed the axisymmetric flow in slender solid propellant rockets with chambers of circular cross-section, where the vorticity shed from the solid propellant surface into the chamber is azimuthal. The analysis of Culick is based on the assumption of self-similarity of the solution with respect to the axial coordinate z, the distance to the non-burning closed wall. With the assumption of incompressible flow the axial velocity component grows linearly with z, and the radial velocity is independent of z. As shown by Balakrishnan et al.[3], the chamber must be slender, $L/a \gg 1$, for the self-similar description to apply, and even in this case the self-similarity breaks down at distances z to the end wall of order a, because the boundary layer due to the radial flow on the end wall separates and leads to a recirculating bubble before reaching the symmetry axis. This is clearly seen in the experiments of Dunlap et al. [4]. In addition, the flow ceases to be self-similar at the open end of the chamber, at distances of order a from the nozzle. Balakrishnan et al. [3] have also shown how to modify the self-similar description when this fails, due to the strong compressibility effects in nozzle-less chambers.

Flandro suggested, see his review paper [5], that the azimuthal vorticity may also play a role in longitudinal acoustic instabilities of axisymmetric solid propellant rockets, because vorticity waves and entropy waves are generated that may effect the nozzle acoustic admittance. The role of these waves in longitudinal acoustic instabilities in axisymmetric rockets was analysed by García-Schäfer and Liñán [6]. Transverse acoustic oscillations could, in principle, induce oscillating longitudinal vorticity. However, as shown by García Schäfer and Liñán[7], the frequencies involved are so high that the axial vorticity is confined to the thin reaction layer adjacent to solid propellant surface.

The description of the quasi-steady flow in slender combustion chambers when the gaseous cavity is not axisymmetric appears to be a formidable problem, involving longitudinal, in addition to the transverse, vorticity; longitudinal vorticity is shed from the propellant surface and amplified due to the stretching effect of the growing axial velocity. Little is known about these flows, although a first attempt to describe the axial vorticity has been carried out by Balachandar et al.[8]. Using the

well justified assumption of incompressibility of the flow, these authors showed that the flow in slender rockets is still self-similar, and wrote the system of equations that govern this flow. They considered that the general problem was not amenable to analysis and, therefore, they restricted their analysis to the case where the internal cylindrical surface of the propellant grain has only small perturbations to the circular cross-section. In this case, a linear perturbation analysis of the basic Culick, axisymmetric, solution can be carried out, showing how axial vorticity is generated, and becomes substantial in a neighbourhood of the chamber center line, due to the bath-tub-vortex effect.

In the present paper we address the general problem of the flow inside star-shaped cylindrical grains, shown in the sketch of Fig.1, when the deviations from circular cross section are not small. The formulation of the self-similar flow is presented in Section 2, where the effects of viscosity are included, and the results of numerical calculations are shown in Section 3 for some representative cases. The main outcome of the results, for star-shaped grains with n lobes, is the generation, due to the stretching of the vorticity by the axial flow, of n pairs of counter-rotating axial vortices, away from the center line of the chamber. In order to analyse the numerical results, the problem is simplified to the Euler equations in Section 4, because in applications, and in the calculations that we have carried out, the Reynolds number of the transverse flow is moderately large compared with unity. The effects of viscosity are taken into account in Section 5 for the description of the asymptotic structure of the core of the vortices. Some final comments are given in Section 6.

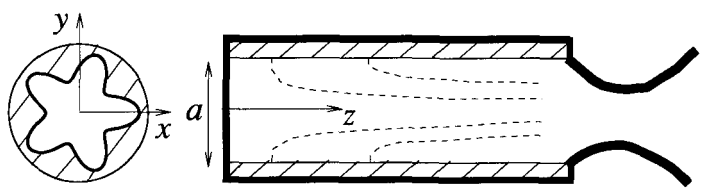

Figure 1. Sketch of the solid propellant combustion chamber, with a star-shaped grain configuration, and the coordinate system.

2. FORMULATION

We consider the flow in a solid propellant rocket with a gaseous cavity bounded by a propellant grain with star-shaped cross-section. Due to the combustion reactions in the thin layers adjacent to the solid-gas interface, a gas flow with constant velocity U_p normal to the propellant surface and a constant temperature T_b appears as generated at the surface. U_p is taken as constant because the Mach number of the flow is small, so that the spatial pressure variations in the chamber are small compared with the pressure p_b at the centre of the closed end of the chamber. Then, we can also consider as constant the density of the gas, $\rho = \rho_b$, and its kinematic viscosity ν_b. In addition, we shall consider that the flow is quasi steady, because the regression

velocity of the solid gas interface is, small compared with U_p by a factor of the order of the ratio ρ_b/ρ_s of the gas and solid densities, which is a small quantity.

For the description of the flow we shall use a system of coordinates, x and y, transverse to the chamber, and the axial coordinate z, measured from the non-reacting closed end wall. The incompressible Navier-Stokes equations have self-similar solutions, in which the transverse velocity components, u and v, are functions only of x and y, and the axial velocity is of the form $w = zW(x,y)$. The pressure p is then of the form $p = p_b - \rho_b(Az)^2/2 + p'(x,y)$.

The equations that describe these self-similar flows are written in non-dimensional form using as scales: U_p for the velocity, $\rho_b U_p^2$ for the pressure variations p', and the characteristic length a of the cross section of the cylindrical cavity for the lengths. In the numerical calculations presented in Section 2, we use as length scale a the radius of a circle with the cross sectional area of the gas chamber. Then the flow equations take the form

$$\frac{\partial u}{\partial x} + \frac{\partial v}{\partial y} + W = 0 \tag{1}$$

$$u\frac{\partial u}{\partial x} + v\frac{\partial u}{\partial y} = -\frac{\partial p'}{\partial x} + \frac{1}{Re}\left(\frac{\partial^2 u}{\partial x^2} + \frac{\partial^2 u}{\partial y^2}\right) \tag{2}$$

$$u\frac{\partial v}{\partial x} + v\frac{\partial v}{\partial y} = -\frac{\partial p'}{\partial y} + \frac{1}{Re}\left(\frac{\partial^2 v}{\partial x^2} + \frac{\partial^2 v}{\partial y^2}\right) \tag{3}$$

$$u\frac{\partial W}{\partial x} + v\frac{\partial W}{\partial y} + W^2 = A^2 + \frac{1}{Re}\left(\frac{\partial^2 W}{\partial x^2} + \frac{\partial^2 W}{\partial y^2}\right) \tag{4}$$

to be solved in the gas domain $C(x,y) < 0$ with the boundary conditions

$$W = 0\,,\ vn_x - un_y = 0,\ un_x + vn_y = -1 \quad \text{at} \quad C(x,y) = 0, \tag{5}$$

corresponding to the conditions of zero tangential velocity and unit normal velocity at the surface; here n_x and n_y are the components of the unit vector $\boldsymbol{n} = \nabla C/\mid \nabla C \mid$ normal to the surface. The constant A^2, corresponding to the axial pressure gradient, independent of x and y, is an eigenvalue of the problem.

We aim for solutions without singularities in the fluid domain; however, we have encountered localized and fairly weak singularities in a finite number of points; see Sections 4 and 5. As indicated before, we can not expect the self-similar description given by the solution of the previous system of equations to be useful if the chamber is not slender. And even if $L/a \gg 1$, the description will fail in two regions of size a, near the end plane and near the nozzle.

Only one parameter, namely, the Reynolds number $Re = aU_p/\nu_b$ is left in the problem. This parameter is large compared with unity for real combustion chambers, so that our calculations and analysis will be aimed to the cases $Re \gg 1$. However we should anticipate that at large values of Re the steady solution will loose stability, forcing us to retain the unsteady effects, represented by the terms $\partial u/\partial t$, $\partial v/\partial t$ and $\partial W/\partial t$ in the left had side of Eqs (2), (3), and (4), respectively. We conjecture that the first instabilities will not modify the self-similar form.

We can anticipate W to be positive, growing form 0 at the solid surface, to a maximum value not larger than A, of order unity. In the continuity equation the axial velocity gradient acts as a continuous distribution of sinks. For this reason we can not introduce directly the stream function $\Psi(x,y)$ of the strictly two dimensional incompressible flows to define the streamlines. However, we can describe

the streamlines of the transverse flow, given by the first of the equations (6), written below, which are the projections on the plane (x, y) of the three-dimensional streamlines that satisfy the equations

$$W\frac{dx}{u} = W\frac{dy}{v} = \frac{dz}{z} \quad , \tag{6}$$

An important ingredient of the solution is the axial vorticity $\Omega(x, y)$ defined by

$$\Omega = \frac{\partial v}{\partial x} - \frac{\partial u}{\partial y} \quad , \tag{7}$$

which satisfies the equation

$$u\frac{\partial \Omega}{\partial x} + v\frac{\partial \Omega}{\partial y} = W\Omega + \frac{1}{Re}\left(\frac{\partial^2 \Omega}{\partial x^2} + \frac{\partial^2 \Omega}{\partial y^2}\right) \tag{8}$$

The first term in the right hand side corresponds to the stretching of the vorticity associated with axial velocity gradient W.

3. NUMERICAL CALCULATIONS

We have solved the steady problem of Eqs (1)-(5) using a finite difference scheme, for some representative cases of star shaped propellant grains, and various Reynolds numbers in the range 100-1000, encountering increasing difficulties at high Reynolds numbers in obtaining the steady solution with the symmetry properties of the star shaped grain. These difficulties may be indicative of the dynamics of the interaction between adjoining vortices.

As a first indication of the results that we obtain, we show in Fig 2 the calculated streamlines, with $Re = 200$, for a star-shaped cavity with five lobes, showing the five pairs of counter-rotating vortices and the dividing streamlines. These streamlines originate at the propellant surface and divide the flow field in domains where the gas appears to reach the center line, or to swirl toward one of the vortices shown in Fig 2. The reader should notice that for a finite length L of the rocket only the fluid particles that leave the propellant surface at a small distance $z \ll L$ will approach the center-line of the chamber or the center of the interior vortices. We show in Fig 3, for one sector, the isolines p' constant, showing negative values in the core of the vortices.

The calculations leading to Fig 3 were carried out using symmetry conditions with the adjoining sectors, but not between the two halves of the sector. We had difficulties to carry out calculations, with this procedure, of the steady flow for values of Re larger than 200; so that we suspect that a bifurcation will be found at some value of Re to an unsteady solution, with the two vortices inside the sector interacting dynamically.

However, it was possible for us to extend the steady calculations to $Re = 1000$ by enforcing the symmetry properties of the flow in the two halves of the sector of Fig 3. These calculations were carried out to investigate the fine structure of the flow at higher Reynolds numbers.

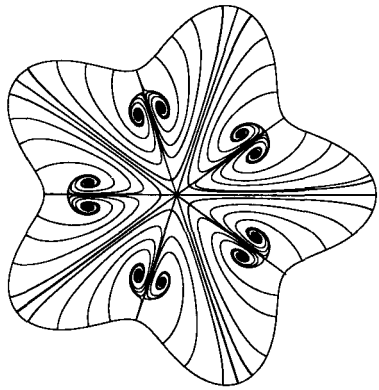

Figure 2. The streamlines calculated for a star-shaped cavity, with $Re = 200$, showing the five pairs of counter-rotating vortices, and the dividing streamlines defining the domain of attraction of the center line and of the vortices.

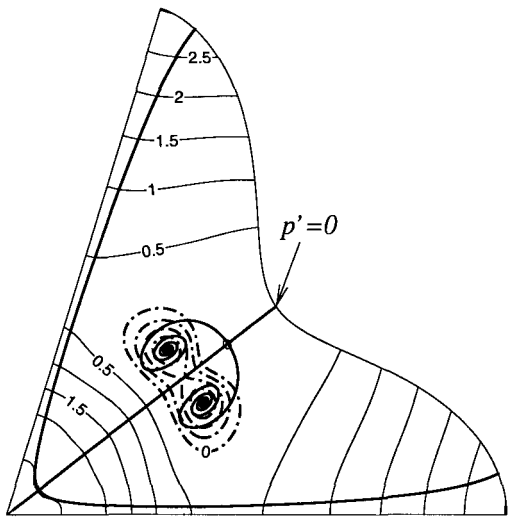

Figure 3. The dividing streamlines for a sector showing the two counter-rotating vortices. Also shown are the line of constant pressure p', with negative values, near the core of the cortices, shown with dashed-dotted lines at intervals 0.2.

Calculations with a fluid flow with the symmetry of the grain configuration can be carried out using a computational domain limited to a half-sector; with the appropriate symmetry conditions at the boundary with the neighbouring half-sectors. The results for $Re = 100$ and $Re = 1000$, and a typical grain configuration, are shown in Figs 4-6. In Fig 5 the dividing streamlines are included because they clarify the flow structure.

In Fig 4 we show the contours of the axial velocity W. The calculated peak values of W are very close to their inviscid asymptotic values, given by the corresponding eigenvalues $A = 4.414$ and $A = 4.357$, for $Re = 10^2$ and $Re = 10^3$. Notice how for $Re = 10^3$ a strong shear layer is formed near the dividing streamlines that separates the gas flow approaching directly the vortex from the propellant surface and the gas reaching the dividing streamline after recirculation. The strong transverse vorticity thus generated at high Reynolds numbers, although lying in a shear layer subject to axial strain, may easily lead to Helmholtz-Kelvin instabilities.

Fig 5 shows, as a more detailed information of the flow field, the streamlines and, with thick lines, the dividing streamlines. Notice first that at the higher values of the Reynolds number only a very small fraction of the gas is directed to the centerline of the chamber; most of the gas tends to recirculate around the vortices. The figure shows how the streamlines tend to converge, due to the axial strain, to the two dividing streamlines that spiral towards the center of the axial vortex. Notice also the significant shift of this center with the Reynolds number.

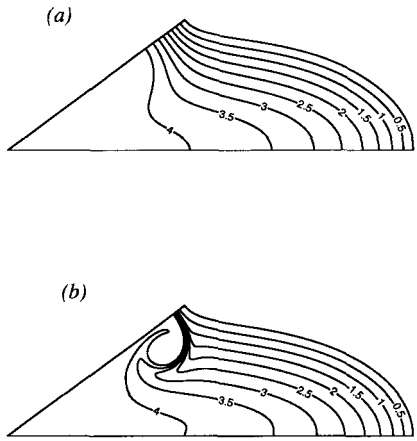

Figure 4. The isolines of the axial velocity W for (a) $Re = 10^2$ and (b) $Re = 10^3$. Notice the strong shear layer in the axial flow at $Re = 10^3$.

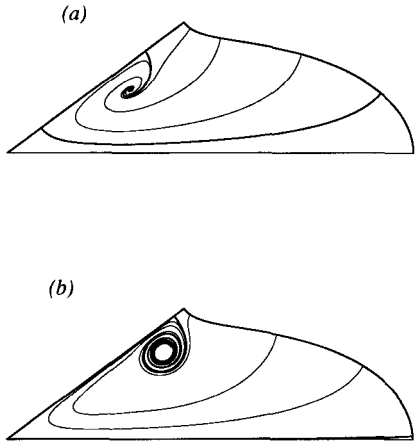

Figure 5. The streamlines, including, with thick lines, the dividing streamlines for (a) $Re = 10^2$ and (b) $Re = 10^3$. Notice that in case (b) most of the flow tends to recirculate around the very strong vortex.

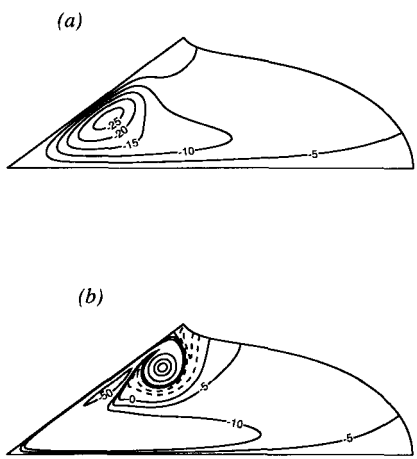

Figure 6. The isolines of the axial vorticity Ω in cases (a), $Re = 10^2$, and (b), $Re = 10^3$. At high Reynolds numbers we find a region outside the dividing streamline with positive vorticity, shown with dashed lines for the values 7.5 and 15.

Fig 6 shows the isolines of constant axial vorticity Ω. For the lower Reynolds numbers, $Re = 10^2$ as an example, the vorticity is of the same sign everywhere; while for $Re = 10^3$ there is a region, close to the dividing streamline, that approaches directly the vortex from the solid surface, with vorticity of a sign opposite to that of the vortex. Notice also the near circular shape of the axial vorticity contours with high value of Ω at the higher Reynolds number. The peak values of the vorticity, although depending on the mesh used in the calculations, scale well with Re. As another example of the generation of axial vorticity, we have analysed the flow in a slender cylindrical chamber, of square cross section, with fluid injection through some porous sections of the walls. The calculated streamlines for $Re = 500$ are shown in Fig 7(a) and the axial velocity iso-contours in Fig 7(b). Notice the four jet-like flows around the eight vortices.

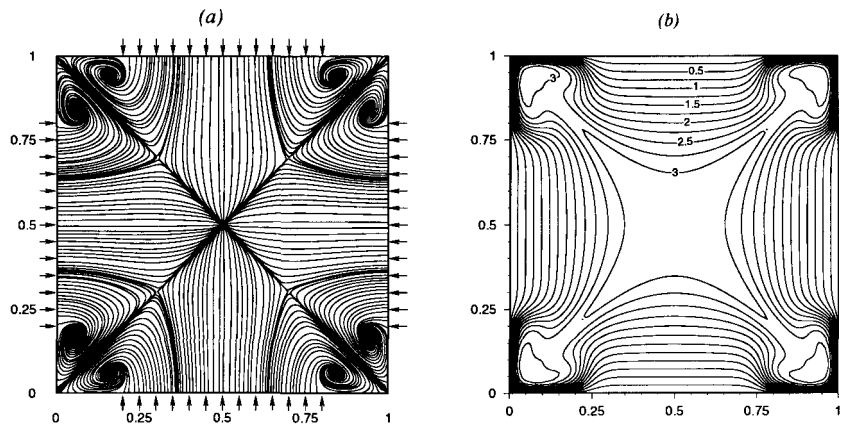

Figure 7. The calculated streamlines (a) and iso-contours of the axial velocity gradient (b), for a slender chamber with injection through porous sections of the walls. The Reynolds number is 500. The velocity gradient is measured with the ratio of the injection velocity and the side of the square.

4. INVISCID FLOW ANALYSIS

Because the Reynolds numbers based on the gasification velocity U_p is $Re \gg 1$, we may expect that the viscous terms are negligible everywhere except in a small neighbourhood of the center line of the vortices, which we shall analyse in Section 5, and also in shear layers along the dividing streamlines. When the viscous terms are dropped from (2)-(4) and (8), these equations are reduced to the Euler equations.

Thus (2) and (3) become

$$u\frac{\partial u}{\partial x} + v\frac{\partial u}{\partial y} = -\frac{\partial p'}{\partial x} \ , \tag{9}$$

$$u\frac{\partial v}{\partial x} + v\frac{\partial v}{\partial y} = -\frac{\partial p'}{\partial y} \ , \tag{10}$$

from which we can derive the equation

$$u\frac{\partial p_0'}{\partial x} + v\frac{\partial p_0'}{\partial y} = 0 \ , \tag{11}$$

which shows that the stagnation pressure $p_0' = p' + (u^2 + v^2)/2$, associated with the transverse flow, is conserved along the streamlines. This p_0' is not uniform because p' varies along the propellant surface.

From (9)-(10) and the definition (7) of the axial vorticity, we obtain the inviscid counterpart of (8)

$$u\frac{\partial \Omega}{\partial x} + v\frac{\partial \Omega}{\partial y} = W\Omega \ . \tag{12}$$

This equation shows how the vorticity grows along the streamlines due to the positive *stretching effect of the axial velocity gradient* W.

In the Euler limit (4) takes the form

$$u\frac{\partial W}{\partial x} + v\frac{\partial W}{\partial y} = A^2 - W^2 \ , \tag{13}$$

which shows that W grows along the streamlines, beginning with the value 0 at the propellant surface, toward the maximum value A.

Equation (13) can be written in the conservative form

$$\frac{\partial}{\partial x}(uW) + \frac{\partial}{\partial y}(vW) = A^2 - 2W^2 \ , \tag{14}$$

which can be used to show, if we take into account our choice of scale a, that the mean value of W^2 is $A^2/2$.

We can also write Eq.(12) in the conservative form

$$\frac{\partial}{\partial x}(u\Omega) + \frac{\partial}{\partial y}(v\Omega) = 0 \ , \tag{15}$$

which allows us to define a stream function $\Psi(x, y) = -p_0'$, because according to (9) and (10)

$$u\Omega = -\frac{\partial p_0'}{\partial y} \quad , \quad v\Omega = \frac{\partial p_0'}{\partial x} \ , \tag{16}$$

and the lines of constant p_0' define the streamlines of the transverse flow.

From Eqs (12) and (13) we can also derive the equation

$$u\frac{\partial}{\partial x}\left\{\Omega\left(A^2 - W^2\right)^{1/2}\right\} + v\frac{\partial}{\partial y}\left\{\Omega\left(A^2 - W^2\right)^{1/2}\right\} = 0 \ , \tag{17}$$

showing that $\Omega(A^2 - W^2)^{1/2}$, like the stagnation pressure $p_0' = p' + (u^2 + v^2)/2$, is conserved along the streamlines. We anticipate that, in the inviscid limit considered here, when the center of the axial vortices encountered in the calculations are approached $W \to A$ and $\Omega \to \infty$, as shown by (13) and (17). Thus, the vortex centers become singular points of the inviscid equations.

5. DESCRIPTION OF THE FLOW IN THE VISCOUS CORE OF A VORTEX

If in the inviscid limit $\Omega \to \infty$ when we approach the center of the vortices we can expect the streamlines to be dominated by the circulating flow associated with the large values of Ω. In this case, for the local flow description, we should use cylindrical coordinates (r, θ), with the origin in the center of the vortex. For values of $r \ll 1$ the neighbouring streamlines, with different origins at the propellant surface, will have different histories, and different values of Ω, v_θ and p_0'. However, at radial distances $r \ll 1$ the circulating velocity will be $v_\theta \gg 1$; the pressure differences must be small while the differences in p_0' are of order unity; as a consequence, the differences in v_θ will be, of order $1/v_\theta$, small compared with unity, and certainly with respect to v_θ. The corresponding radial oscillations of Ω will also be small, even before the viscosity will act, for values of $r \sim 1/\sqrt{Re}$, to exchange vorticity between neighbouring streamlines so that Ω is smoothed to a function only of r. In the region $r \sim 1/\sqrt{Re}$, we conjecture that the flow field can be approximated by

$$v_r = v_r(r)\,, v_\theta = v_\theta(r) \quad \text{and} \quad W = A\ . \tag{18}$$

so that from the simplified form of the contiuity equation

$$\frac{1}{r}\frac{\partial}{\partial r}(rv_r) = -A\ , \tag{19}$$

we obtain

$$v_r = -\frac{A}{2}r \tag{20}$$

The axial vorticity equation (8) will take the form

$$-\frac{1}{2}Ar\frac{\partial \Omega}{\partial r} = A\Omega + Re^{-1}\frac{1}{r}\frac{\partial}{\partial r}\left(r\frac{\partial \Omega}{\partial r}\right) \tag{21}$$

with Ω defined in terms of v_θ by

$$\Omega = \frac{1}{r}\frac{\partial}{\partial r}(rv_\theta) \tag{22}$$

Eq.(21) is the well known equation describing the vorticity distribution in a Burgers strained vortex.

We can scale r with $r_c = (ARe)^{-1/2}$, defining $\xi = r/r_c$, to eliminate A and Re from (21), so that we obtain the equation

$$-\frac{1}{2}\xi\frac{d\Omega}{d\xi} = \Omega + \frac{1}{\xi}\frac{d}{d\xi}\left(\xi\frac{d\Omega}{d\xi}\right) \tag{23}$$

which is to be solved with the far field condition that for $\xi \gg 1$, Ω does not blow up. Then, the solution $\Omega(\xi)$ takes the form

$$\Omega/Re = c_1 exp(-\xi^2/4) + c_2\Phi(\xi) \tag{24}$$

where

$$\Phi(\xi) = exp(-\xi^2/4)\int_1^\xi x^{-1}exp(x^2/4)dx \tag{25}$$

The constants c_1 and c_2, of order one, must be obtained as part of the complete numerical solution. The constant c_2 is $c_2 \equiv 0$ in the Burgers solution for the strained vortex, but it may be non zero if the farfield has vorticity originating at the surface. For large values of ξ, Ω/Re is given by $c_2\Phi(\xi)$, where

$$\Phi(\xi) \to 2/\xi^2 \quad \text{when} \quad \xi \to \infty\,, \tag{26}$$

while

$$\Phi(\xi) \to -0.13326 + \ln(\xi) \quad \text{for} \quad \xi \to 0 \tag{27}$$

Then

$$\Omega/Re \to c_1 + c_2[-0.13326 + \ln(\xi)] \quad \text{for} \quad \xi \to 0 \tag{28}$$

Thus the results show a logarithmic singularity of Ω at $r \to 0$, implying a vorticity sink at $r = 0$, and also show a weak integrable singularity when we try to calculate the tangential velocity v_θ using (22). However, our preliminary numerical results are consistent with a value $c_2 = 0$ and a value $c_1 = -0.302$ for $Re = 10^3$, corresponding to a vortex circulation $\Gamma = 4\pi c_1/A = -0.896$.

6. CONCLUDING COMMENTS

The numerical calculations that we have carried out for the non-asisymmetric high Reynolds number flow in the slender gaseous cavities of solid propellant rockets show a complicated flow field, involving transverse and axial vorticity originating at the propellant surface, where there is no boundary layer because it has been blown-off by the gasification flow. The axial vorticity is amplified by the stretching effect of the increasing axial velocity along the chamber. The vorticity tends to concentrate in axial vortices positioned away from the center line of the chamber. For star-shaped solid propellant grains with n lobes, we find n counter rotating vortex pairs that dominate the flow field. They will interact dynamically in an unsteady way at the highest Reynolds numbers at which computations have been carried out, thus contributing to the acoustic instabilities in the chamber. Because the flow Reynolds numbers are large, we have carried out a preliminary analysis based on the Euler equations, which needs much more refinement and future work. The analysis of the inviscid flow leads to the appearance of shear layers, placed along the dividing streamlines, in addition to the concentrated regions of high axial vorticity Ω, which grows with the inverse of the square of the distance r to the center of the vortex. We show how the viscous effects change the growth of Ω from $2c_2/r^2$ to a form for Ω/Re in terms of $\xi = rRe^{1/2}$, with a weak singular dependence $\ln r$ on r.

The equation (21) that describes the viscous core structure is the equation obtained by Burger for the structure of a vortex subject to axial strain. The Burgers solution corresponds to the first term in (24), with $c_2 \equiv 0$. It is the second term the one that leads to the $\ln r$ singularity in Ω. It is a consequence of the amplified vorticity, with an algebraic behaviour, $1/r^2$, in r, that originates in the far field.

The resulting singularity, inside the flow field, of the self-similar solution of the Navier Stokes equations may, however, disappear when we account for the viscous effects in the closed end wall of the chamber, where the flow is not self-similar. It turns out that the fluid particles that may approach the center line of the vortices, with $r \ll 1$, must have left the lateral surface of the solid propellant at very small values of z, as can be derived from (6). Thereby, these fluid particles come from the end wall boundary layer, affected by non self-similar effects that may modify the

viscous core structure but not the intermediate region where $\Omega r^2 \approx 2c_2$. However, our numerical results suggest c_2 to be equal to zero, associated with localized vortices of circulation $\Gamma = 4\pi c_1/A$, weakly dependent on the Reynolds number.

Acknowledgment

The work carried out by A.L. and V.K. has been supported by the MCYT under Project C02013002. V.K. acknowledges also the financial support of the MCYT through the Ramón y Cajal Program.

REFERENCES

[1] G. I. Taylor, Fluid flow in regions bounded by porous surfaces. *Proc. R. Soc. London A* **234**, 456–475 (1956).

[2] F. E. Culick, Rotational asisymmetric mean flow and damping of acoustic waves in solid propellent rockets. *AIAA J.* **4**, 1462–1464 (1996).

[3] G. Balakrishnan, A. Liñán and F.A. Williams, Rotational inviscid flow in laterally burning solid propellant rocket motors. *J. Propulsion Power* **8**, 1167–1176 (1992).

[4] R. Dunlap, P. G. Willoughby and R. W. Hermsen, Flow field in the combustion chamber of a solid propellant motor. *AIAA J.* **12**, 1440–1441 (1974).

[5] G. A. Flandro, Effects of vorticity on rocket combustion stability. *J. Propulsion Power* **11**, 607–625 (1995).

[6] J. E. García Schäfer and A. Liñán, Longitudinal acoustic instabilities in slender solid propellant rockets: linear analysis. *J. Fluid Mech.* **437**, 229–254 (2001).

[7] J. E. García Schäfer and A. Liñán, Transverse acoustic instabilities in slender solid propellant rockets: linear analysis. *Trans. Tenth International Congress on Sound and Vibration.* 7-9 July, Stockholm, Sweden (2003).

[8] S. Balachandar, J. D. Buckmaster and M. Short, The generation of axial vorticity in solid-propellant rocket-motor flows. *J. Fluid Mech.* **429**, 283-305 (2001).